drones

Article

Automatic recognition of Black-necked Swan (*Cygnus melancoryphus*) from UAV imagery

Marina Jiménez-Torres [1,2,3,4]*, Carmen P. Silva[3], Carlos Riquelme[5,6], Sergio Estay[3,6] and Mauricio Soto-Gamboa[1,3,4]*

[1] Laboratorio de Ecología Conductual y Conservación, Instituto de Ciencias Ambientales y Evolutivas, Facultad de Ciencias, Universidad Austral de Chile; mrsoto@uach.cl
[2] Programa de Doctorado en Ciencias mención Ecología y Evolución, Escuela de Graduados, Facultad de Ciencias, Universidad Austral de Chile, Valdivia, Chile; secgrad@uach.cl
[3] Instituto de Ciencias Ambientales y Evolutivas, Facultad de Ciencias, Universidad Austral de Chile. Valdivia, Chile; Inst.C.A.Ev@uach.cl
[4] Programa Austral-Patagonia, Universidad Austral de Chile.
[5] Doctorado en Ciencias Biológicas mención Ecología, Pontificia Universidad Católica de Chile; cgriquelme1@uc.cl
[6] Center of Applied Ecology and Sustainability (CAPES), Pontificia Universidad Católica de Chile, Santiago, Chile; sergio.estay@uach.cl
* Correspondence: mrsoto@uach.cl (M.S.); marina.jimenez.torres@alumnos.uach.cl (M.J); Tel.: +56 63 2293044 (M.S)

Citation: Jiménez-Torres, M.; Silva, C.; Riquelme, C.; Estay, S.; Soto-Gamboa, M. Automatic recognition of Black-necked Swan (*Cygnus melan-coryphus)* from UAV imagery. *Drones* **2022**, *6*, x. https://doi.org/10.3390/xxxxx

Academic Editor: Firstname Lastname

Received: date
Accepted: date
Published: date

Abstract: The use of drones in animal monitoring programs has two significant limitations. First, the increase of information requires a high capacity of storage, and second, time invested in data analysis. We present a protocol to develop an automatic object recognizer to minimize analysis time and optimize data storage. We used a Black-necked swan (*Cygnus melancoryphus*) as a model because it is abundant and has a contrasting color compared to the environment, making it easy detection. We conducted this study at the Cruces River, Valdivia, Chile, using a Phantom 3 Advanced drone with an HD-standard camera. The drone flew 100 m obtaining georeferenced images with 75% overlap and developing approximately 0.69 km2 orthomosaics images. To build the recognizer, we estimated the swans' spectral signature and adjusted nine criteria for object-oriented classification. We obtained 140 orthophotos classified into three brightness categories. We found a Precision, Sensitivity, Specificity, and Accuracy higher than 0.93 and a calibration curve with R2= 0.991 for images without brightness. The recognizer prediction decreases with brightness but is corrected using ND8-16 filter lens. We discuss the importance of this recognizer to data analysis optimization and the advantage of using this recognition protocol for any object in ecological studies.

Keywords: Automatic recognition; UAV; Black-necked swan; Abundance and density estimation; orthomosaic object recognition

1. Introduction

Ecological monitoring programs are essential to understanding the population dynamics of different species worldwide. These monitoring programs allow researchers to describe natural patterns or detect disturbances, generating information to develop efficient management tools and knowledge-based decision-making [1-4]. New technologies improve the data collection quantity and quality from natural systems, increasing the precision and exactitude of measures to establish better monitoring programs [4,5]. Remote sensing techniques allow obtaining information from isolated places, reducing sampling time and effort, and increasing the collected information's Accuracy [6,7]. Additionally, remote sensing can provide consistent long-term observation data at different scales, from local to global [8]. The information generated from these remote sensors depends on the sensor incorporated and on the characteristics of the images it produces, like a) spatial resolution (pixel size), b) spectral resolution (wavelength ranges), c) temporal resolution (when and how often images are collected), and d) spatial extent (ground area represented) [9].

Unmanned Aerial Vehicles (UAV) or drones have rapidly grown over the years because of their accessibility, low-cost operation, versatility in size, flight autonomy, and the type of information they can collect [10,11]. This approach has been increasing the number of applications, including monitoring processes in agriculture, forestry, and ecology [12-18]. In this sense, monitoring programs have benefited from drones' advantages, mainly because of the replicability of flight paths and the lower sampling effort, making more attainable time-series data [16]

Although the use of drones improves the accuracy of the spatial information obtained [19, 5, 20], the increase in data collection and the time invested in data analysis can turn into a significant disadvantage [21,19, 22]. In response to this problem, automation in the processing and analyzing of images is a recent and promising research area [23]. This process generates multiple benefits, mainly reducing the time invested in analyzing photographs and videos and reducing or eliminating the bias generated by the observer [22]. Being an automatic process, it has the potential to be standardized and replicable [21]. Also, most of the parameters in the algorithms can be modified and used with different UAVs, focal species, and research for various purposes [21].

Most automatic recognition methods involve the use of spectral properties [24]; pattern recognition (i.e., shape and texture; [25]), and the use of filters to increase the contrast between the object of interest and the background [26]. These methods allow the systematic monitoring of multiple species and reduce the analysis time [27], optimizing the early detection of wildlife changes and contributing to evaluating conservation measures' effectiveness [7]. This study develops and describes an automatic count protocol of black-necked swans (*Cygnus melancoryphus*) under natural conditions. We used UAV imagery and supervised classification methods to establish the spectral signature of black-necked swans and the shape attributes and propose this protocol as a tool for automatic classification of any object (individual) to be recognized from UAV imaginary.

Materials and Methods

2.1 Model and study area

The black-necked swan is an aquatic bird of the Anatidae family and the only species of the genus Cygnus in the Neotropics [28]. Its distribution includes Argentina, Chile, Uruguay, and southern Brazil [28, 29]. This species is a medium size (5-7 kg) herbivorous bird whose diet is strongly related to the consumption of *Egeria densa* [30]. Black-necked swans are highly social and gregarious outside the breeding season, between July and March [31]. In the IUCN Red List of Threatened Species [29], the black-necked swan is classified as Least Concern, but the Chilean classification has different conservation status categories (Endangered and Vulnerable). In the study site, the black-neck swan is classified as Endangered.

We carried out this study at the Carlos Anwandter Sanctuary (39º49'S, 73º15'W), a 48.8 km² coastal wetland located in the southern range of the Valdivian Temperate Rain Forests Ecoregion, Chile [32, 33]. In addition, we incorporated two sites in the Cruces River close to Valdivia city (Figure 1). We selected three sites where we performed 110 survey missions (48 for site 1, 44 for site 2, and 18 for site 3) between July 2017 and October 2018, using a Phantom 3 Advanced drone, with an HD standard camera recorder (Sony Exmor R BSI 1/2.3" sensor with 12 MP). We obtained the image following a pre-established back-and-forth route (transect) using the MyPilot application (https://www.mypilotapps.com). The drone flew 100 m above the water mirror level, obtaining georeferenced images with 75% overlap at both axes for orthophotograph construction (Figure 2). During each survey, we obtained 370 ± 90 (mean±1 SD) images with a surface of 0.69 km2 by image and a pixel resolution of 3.854± 0.135 (mean±1 SD) cm. For orthophotograph construction, each set of images (one set for the survey mission) was mosaiced using an online version of the Dronedeploy software (https://www.dronedeploy.com). Orthophotos are composed of 3 bands: red, green, and blue (RGB color model) within the visible spectrum (740 to 380 nm λ).

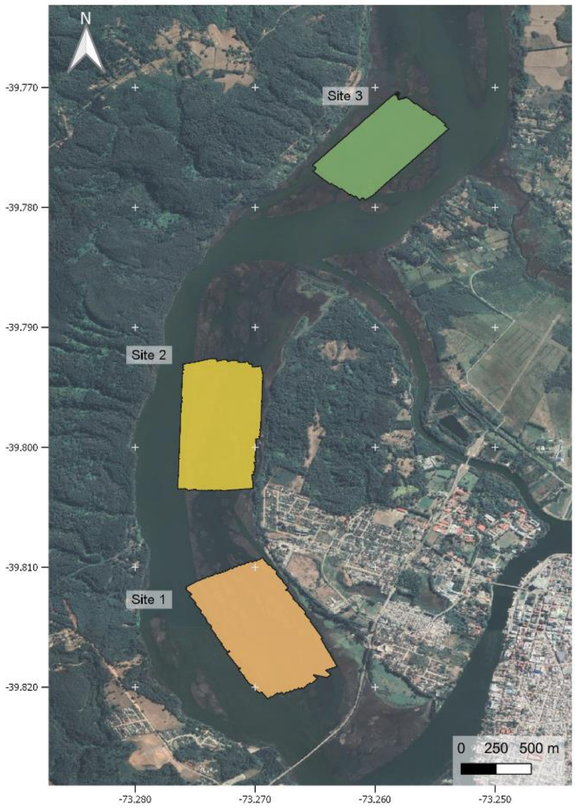

Figure 1. Study area. Geographic location of the study area. The area within squares represents each sampling site, orange corresponds to site 1, yellow corresponds to site 2 and green corresponds to site 3.

2.2 Building the recognizer

The first step in developing the automatic recognizer was to describe the black-necked swans' spectral signature. We randomly selected 14 out of 110 orthophotos, and we manually selected ten individuals (140 total) for each. We recorded the range of spectral values for each pixel in each band for each selected individual. We determined the minimum threshold value for defining a black-necked swan in a band as the first quartile of the distribution of the spectral values in each band. According to the previous configuration, we filtered each orthophoto. If the pixel shows values higher than the threshold in all bands, it was classified as 1 and 0 otherwise. Finally, we vectorized the raster obtaining a vector layer where each polygon represents a swan.

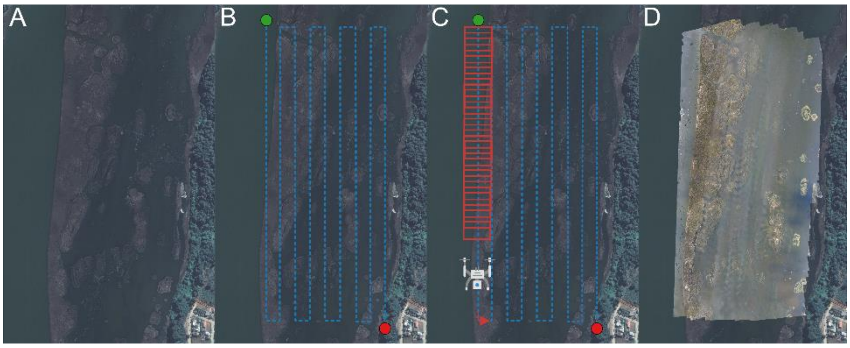

Figure 2. Steps for obtaining orthophotographs. (**a**) Example for the sampling site number 2, (**b**) the design of the flight transects, (**c**) the superimposition of the obtained images and (**d**) the creation of the orthophotography in the DroneDeploy software.

In a second step, we established an Object-oriented classification. We selected nine attributes of the shape. We classified these measures into three groups, following a hierarchical procedure from groups 1 to 3. Group 1 included polygons: a) Size, b) Perimeter, c) Area/Perimeter ratio, and d) Shape index, defined as $((4\pi^{*}\ \text{Area}) / (\text{Perimeter}^2))$, where values close to 0 correspond to more prolonged and thinner figures, and values close to 1 resemble a circle [34]. Group 2 included a) Box's length, the minimum bounding box's length that contains the polygon, b) Box's wide, the minimum bounding box's width that contains the polygon, and c) Box's Length/Width, i.e., the quotient between the length and the width of the box, and d) Intersection area, corresponds to the percentage of the box intersected by the object. Group 3 included a) Vertices number of the polygon. To optimize the procedure, we used the first 14 orthophotos (140 individuals) and considered each measure's maximum and minimum value to incorporate in the recognizer.

2.3 Evaluating the accuracy of the recognizer and confusion matrix

Using the results from the previous steps, we applied the filter to the remaining 96 orthophotos to obtain the number and spatial position of the classified "swans" objects. We performed the analyses using QGis 2.18 [35] and the R software [36], including the packages Raster [37], rgdal [38], geosphere [39], spatstat [40], maptools [41], gdalUtils [42], rgeos [43], spatialEco [44] and R.utils [45]. We include the R code for the analysis in the supplementary material (SM).

Due to the water brightness, overexposed or badly reconstructed areas can appear in orthophotos; we classified the orthophotos into three classes following Chabot and Francis (2016) [22]: a) 0, there was no brightness, b) 1, there was localized brightness, and c) 2, the brightness was present throughout the orthophoto (Figure 3). We performed an independent analysis for each of the three categories.

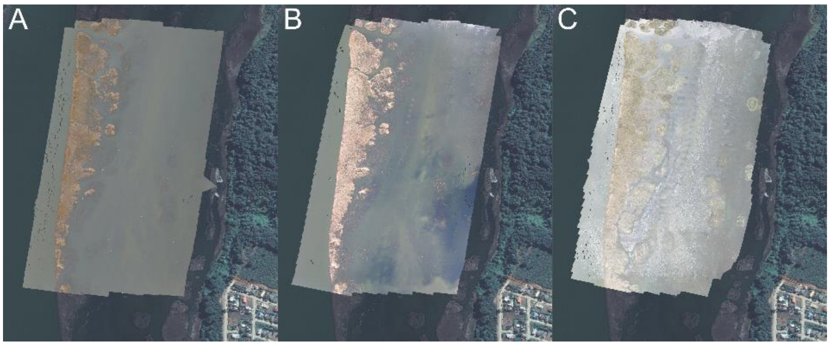

Figure 3. Brightness orthophoto classification. (**a**) Category 0, there was no brightness, (**b**) Category 1, there was localized brightness, and (**c**) Category 2, the brightness was present throughout the orthophoto.

To evaluate the validity of the filtering procedures, we constructed a confusion matrix [46]. We manually checked all objects recognized by the filters in each of the 96 orthophotographs. We estimate True-Positive object (TP) as the object correctly assigned as black-necked swans; False-Positive object (FP), corresponding not black-necked swans object, that recognizer assigned as swans; and False-Negative (FN), missing black-necked swans archived in the orthophoto, but not recognized by the recognizer. In addition, we estimated the true negative as the number of objects recognized by the spectral signature but rejected by the shape filters (TN). We estimated confusing matrix indicators including: Precision = TP/(TP + FP), Sensitivity = TP/(TP + FN), Specificity = TN/(TN + FP), and Accuracy = (TP + TN)/(TP + TN + FP + FN). Finally, we compared the manual count and recorder estimates in each orthophoto classification fitting linear regression model using R software [36].

3. Results

3.1.1 Filtering process

The minimum critical thresholds for the black-necked swans' coloration corresponded to 220 for the red, 221 for the green, and 221 for the blue bands (Figure 4). We summarized the specific range estimated for each shape attributed in Table 1.

Table 1. Shape attribute values. Lower and upper limit of the range in which an object is classified as a Swan for each shape attribute used in the recognizer.

Shape attributed	Lower limit	Upper limit
Size	0.0111562	0.5501689
Perimeter	0.6220029	4.8082500
Area/Perimeter ratio	0.0179360	0.1476506
Shape index	0.2166254	0.6981190
Box's length	0.2144787	1.1876790
Box's wide	0.1367180	0.8679846
Box's Length/Width	1.0001040	3.7119470
Intersection area	30.7244900	88.3788400
Vertices	11	72

3.1.2 Confusion matrix

Concerning the brightness of the images, we classified 29 orthophotos in category 0, 14 in category 1, and 67 in category 2, representing 26.4 %, 12.7%, and 60.9%, respectively. From the 29 orthophotos classified as category 0, the recognizer found a total of 17345 objects, while by direct count, we found 16940 black-necked swans. In this case, the Precision, Sensitivity, Specificity, and Accuracy were higher than 0.93 (Table 2). In the 14 orthophotos classified as category 1, the recognizer found 10345 objects, while we estimated 7228 individuals by direct count. Sensitivity, Specificity, and Accuracy remained at high values (<0.90), but the Precision decreased to 0.687 (Table 2). The recognizer in category 2 orthophotos assigned 757958 objects as black-necked swans, while we estimated 26584 individuals by manual count. Precision decreased at 0.033, showing very bad object estimations (Table 2). In this case, the recognizer overestimates the FP, assigning a high number of brightness spots as Black-necked swans individuals. Sensitivity remains at high values, but Specificity and Accuracy decrease to values nearest to 0.82 (Table 2).

Table 2. Confusion matrix parameters for each brightness category

	Brightness		
	Category 0	**Category 1**	**Category 2**
Precision	0.948	0.687	0.033
Sensitivity	0.973	0.987	0.964
Specificity	0.99	0.96	0.82
Accuracy	0.988	0.962	0.827

In relation to recognized predictive capacity, we found high level of accuracy in orthophotos classified as category 0 (slope =0.97, intercept= 0, adjusted R^2= 0.991, Figure 4a). In category 1, we found equivalent results, but with a tendency of overestimates abundance (slope= 1.33, intercept=0, adjusted R^2= 0.989, Figure 4b). Finally, we found no significant linear regression between manual recount and recognizer in orthophotos classified as Category 2, indicating recognized non-accuracy for this brightness image (Figure 4c).

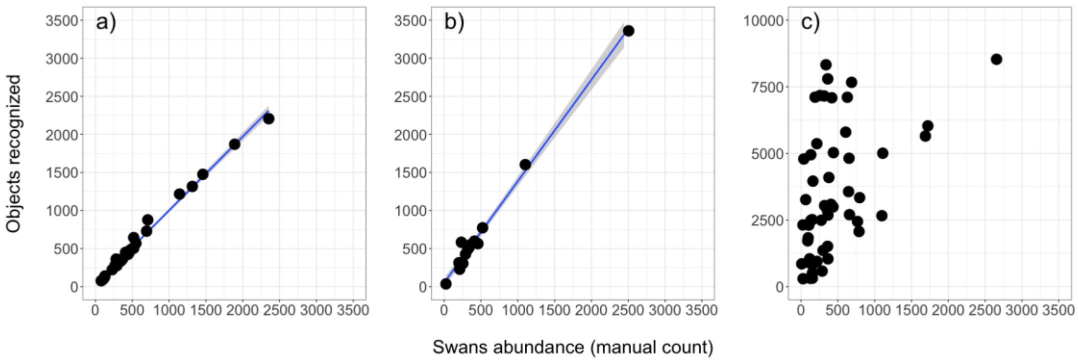

Figure 4. Recognizer predictivity capacity. We show the linear regression results between absolute abundance (manual count) and the object automatically recognized. The blue line represents the linear model, and the gray confidence interval uses standard error. In (a), We present the results of orthophotos without brightness (category 0), (b) moderate brightness (category 1), and (c) high brightness levels (category 2).

4. Discussion

We optimized a filtering protocol to establish an automatized system for counting black-necked swans from orthophotos. We analyzed 110 orthophotographs and compared manual versus automatized procedures to do this. We quantified 50752 swans by manual count, whereas the automatic recognizer estimated a total of 49262, which missed only 1653 swans (representing 3.257 % of individuals lost). The spectral filter lost 163 individuals associated with the object's size. In this case, we mainly lost chicks represented by a few pixels. Consequently, we found that the spectral signature was altered with environmental borders because the low number of pixels with the objects is recognized.

We identified eight situations where the recognizer fails: i) When two individuals are extremely close, the spectral signature cannot separate individuals (n=251 individuals). In this case, the shape filter excludes both individuals (Figure 5a). ii) Two individuals are extremely close and present different sizes (n=257). The spectral filter recognizes only one individual, and then the shape filter recognizes it; thus, only one individual is lost (Figure 5b). iii) young swans (n=417 individuals). We optimized the filter to recognize adult shapes and sizes; thus, young swans are discarded (Figure 5c). iv) Familiar groups (n=68 individuals). When all swans are close together, the shape filter discards all the individuals (Figure 5d). v) adults cluster (n=44 individuals). In some cases, swans swim in line very close to each other (from 3 to 8 individuals), and the shape filter discards the object, losing all the individuals (Figure 5e). vi) Swans in wetland vegetation (n=85 individuals). We observed that grassland distorts swans' shape, and the shape filter rejects these objects (Figure 5f). vii) Flying swans (n=8 individuals); extended wing changes the object's shape, and the shape filter rejects it (Figure 5g). viii) Orthomoisaic reconstruction (n=360 individuals). In some cases, especially in borders, orthophotos present deformations, seams, or gaps affecting swan shape; therefore, the shape filter rejects the objects (Figure 5h).

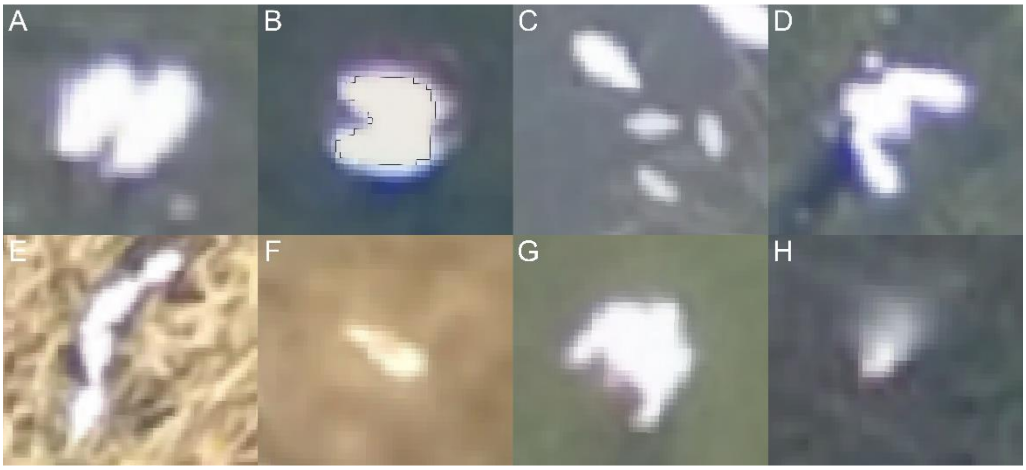

Figure 5. False negative objects. Causes of Unrecognized Black-necked swan. (**a**) Two black-necked swans close together (lost both), (**b**) individual proximity (lost one), (**c**) juvenile or young swans, (**d**) familiar groups, (**e**) adults cluster, (**f**) Swans in wetland vegetation, (**g**) flying swans, (**h**) Image swan deformations.

In orthophotos classified in category 0, we obtained near 6.1% of error in the swan identifications, similar to other works in birds and marine mammals [21,22,47]. Most automatized recognizers only analyze the identification accuracy concerning manual counts but do not perform a confusion matrix; therefore, they are not evaluating the effectiveness of the recognizers [48, 21, 18, 49]. Moreover, in most cases, the studies complete the recognizer with raw data without error classification omitting availability, perception, misidentification, and double counting, among others [17, 48, 50, 51, 52]. By incorporating the description of the types of error and their quantification, we can know the recognizer's reliability, and we could be modified the spectral and shape parameters to increase the accuracy or establish reliability intervals.

We must point out that the brightness directly affects spectral classification and overestimates false positive objects. In general, when attempting to identify bright or white birds (i.e., black-necked swans), the most difficult elements to remove/discriminate are those related to the color white, such as glitter, flashes, and foam in the water or pale rocks, as they are very similar to the object of interest [52, 22]. Other water factors such as waves, sunshine, or water movement generates brightness in the orthophotos failing in the correct object assignation or directly affecting the orthophoto construction by missing image overlapping lost meeting points [49, 22]. In our case, we obtained an overestimated black-necked swan abundance, directly associated with brightness, causing an increase of false positives and the error in identification by decreasing Accuracy and Sensitivity [49]. A similar problem was described using a thermal camera where the rock heath emission in the forest floor produces false-positive heath points similar to warm blood animals [53, 54, 55]. We suggest eliminating false positives manually for these cases, mainly if they are concentrated in specific areas of the orthophoto, such as bright spots [22]. We found that brightness is generated mainly at the orthophoto edges, so we recommend increasing the sampling area. An alternative solution is incorporating a polarizer lent to the drone's camera. In our case, we used an ND8 filter lent (we recommended ND8 or 16). Therefore, using a polarizer or color-correcting lent can help avoid over or under-light exposition and increase the contrast between object and environment. Using these elements permits avoiding the possible errors associated with climate variables and expanding flight schedules.

The flight transects design can influence the correct orthophotos assembly; a wrong orientation of the transect can generate that an animal in movement may be captured in two adjacent photos, which could cause a double count of the same individual (false positives; [56]). A low percentage of overlapping images does not present enough meeting points between adjacent images, generating spaces without data that do not represent the terrain's reality or the appearance of shadows and shadows within the surface [22]. The literature recommended that the minimum overlap percentage to reconstruct any surface is 60% [57]. We used a 75% overlap during the first stage of sampling; later, we increased it to 80%, overlapping percentage suggested when reconstructing water, snow, and clouds, or surfaces with fewer meeting points due to their color or texture, or constant movement [22]. Drone movements, because of the wind, can also reduce the percentage of overlap between images. In some cases, wind can cause a 5 to 37% loss overlap when using 57% of overlapping [58]. In extreme cases, the wing instability produces the loss of the nadir position (the perpendicular line between the camera and the surface), causing inconsistencies between the objects' size and shape [58, 22].

We observed an increase in these errors during the breeding and rearing season. First, adults are closer together, especially breeding pairs or familiar groups. Second, black-necked swans build nests on the reed beds, and incubation is exclusively for females while males guard the nest [31]. During this period, individuals spend most of their time on the wetland vegetation, hindering automatic recognition. To avoid these complications, we recommend a post-manual inspection, or as has been suggested, an increase of temporal replications or complement the automatic counting with direct observations [56]. Another option to increase the accuracy of this procedure is to build a specific recognizer for aggregations. For example, in the grey seal (*Halichoerus grypus*), where the aggregations are of six or more individuals, Convex Envelopes over the polygons were made to discriminate between individuals and aggregations, where depending on the size of the aggregation, the number of individuals was determined [59]. In other cases, authors have used the number of pixels as a size approximation to discriminate between bird aggregations [26].

Aerial drone sampling is a more effective alternative to traditional sampling when monitoring birds, especially waterfowl, obtaining more accurate counts than those made by direct counts [20, 51]. Drones have been used to quantify birds' abundance under-sensitive to observer-generated disturbances, birds concentrated in small areas (colonies or flocks), birds inhabiting open habitats, and birds that contrast strongly with the background and other image elements [22]. Our work established an automatized protocol, increasing object detection accuracy and reducing the time spent on image processing. We calculated effectiveness indices using the automatized procedures, recorded the different types of errors, and improved image analysis. Although we optimized the recognizer for the black-necked swan's classification, the steps we described are a procedure that can be generalized. It can be applied to any object recognized (animals, plants, mobile or stationary objects). For example, we applied the same protocol to estimate the abundance of red-gartered coot (*Fulica armillata*). In this case, the birds' black general coloration does not permit the implementation of an efficient spectral signal filter. To solve this problem, we use a negative photographic technique to obtain a similar white spectral signature to the black-necked swans. Therefore, we increased the spectral signature resolution by modifying the orthophoto's original coloration spectral to achieve the best environmental/object contrast.

Automated recognizers are essential to establish long-term animal monitoring aerial surveys. We propose the following steps i) building an orthomosaic image to construct efficient automated recognizers. ii) spectral signal definition, if necessary, modify the original image coloration to obtain the best environmental/object contrast, iii) establish an Object-oriented classification based on shape, iv) perform a Confusion analysis to estimate the accuracy (and the improvement possibility) of the recognizer, and v) manual supervision to estimate the number of missing objects.

Supplementary Materials: The following supporting information can be downloaded at: www.mdpi.com/xxx/s1

Author Contributions: Conceptualization, M.J.T. and M.S.G.; writing, M.J.T., M.S.G., C.P.S.; Data curation M.J.T; Formal Analysis, M.J.T., C.R., S.E. and M.S.G.; Founding acquisition, M.S.G. All authors have read and agreed to the published version of the manuscript.

Funding: This research was partially funded by the Dirección de Investigación, Vicerrectoría de Investiagación y Creación Artística, Universidad Austral de Chile.

Data Availability Statement: Not applicable

Acknowledgments: Marina Jiménez Torres is supported by ANID-Subdirección de Capital Humano/Doctorado Nacional/2022-21221530.

Conflicts of Interest: The authors declare no conflict of interest.

References

1. Siddig, A.; Ellison, A.; Ochs, A.; Villar-Leeman, C.; Lau, M. How do ecologists select and use indicator species to monitor ecological change? Insights from 14 years of publication in Ecological Indicators. *Ecol Indic.* **2016**, *60*, 223-230.
2. Young, J., Murray, K., Strindberg, S., Buuveibaatar, B., Berger, J. Population estimates of endangered mongolian saiga *Saiga tatarica mongolica*: Implication for effective monitoring and population recovert. *Oryx.* **2010**, *44*, 285-292.
3. Collen, B., McRae, L., Deinet, S., De Palma, A., Carranza, T., Cooper, N., Loh, J., Baillie, J. Predicting how populations decline to extinction. *Phil Trans Royal Soc London B.* **2011**, *366*, 2577-2586.
4. Hollings, T., Burgman, M., van Andel, M., Gilbert, M., Robinson, T., Robinson, A. How do you find the green sheep? A critical review of the use of remotely sensed imagery to detect and count animals. *Methods Ecol evol.* **2018**, *9*, 881-892.
5. González, L., Montes, G., Puig, E., Johnson, S., Mengersen, K., Gaston, K. Unmanned aerial vehicles (UAVs) and artificial intelligence revolutionizing wildlife monitoring and conservation. *Sensors.* **2016**, *16*, 97.
6. Kerr, J., Ostrovsky, M. From space to species: Ecological applications for remote sensing. *Trends Ecol. Evol.* **2013**, *18*, 299–305.
7. Rose, R., Byler, D., Eastman, J., Fleishman, E., Geller, G., Goetz, S., Guild, L., Hamiltom, H., Hansen, M., Headley, R., Hewson, J., Horning, N., Kaplin, B., Laporte, N., Leidner, A., Leimgruber, P., Morisette, J., Musinsky, J., Pintea, L., Prados, A., Radeloff, V., Rowen, M., Saatchi, S., Schill, S., Tabor, K., Turner, W., Vodacek, A., Vogelman, J., Wegmann, M., Wilkie, D., Wilson, C. Ten ways remote sensing can contribute to conservation. *Conserv. Biol*. **2015**, *29*, 350–359.
8. Wang, K., Franklin, S. E., Guo, X., Cattet, M. Remote sensing of ecology, biodiversity and conservation: a review from the perspective of remote sensing specialists. *Sensors*. **2010**, *10*, 9647-9667.
9. Turner, W., Spector, S., Gardiner, E., Flandeland, M., Sterling, E., Steininger, M. Remote sensing for biodiversity science and conservation. *Trends Ecol. Evol*. **2003**, *18*, 306-314.
10. Hildmann, H., Kovacs, E. Using unmanned aerial vehicles (UAVs) as mobile sensing platforms (MSPs) for disaster response, civil security and public safety. *Drones.* **2019**, *3*, 59.
11. Yao, H., Qin, R., Chen, X. Unmanned aerial vehicle for remote sensing applications—A review. *Remote Sens.* **2019**, *11*, 1443.
12. Abd-Elrahman, A., Pearlstine, L., Percival, H. Development of pattern recognition algorithm for automatic bird detection from unmanned aerial vehicle imagery. *Surv. Land Inf. Sci*. **2005**, *65*, 37–45.
13. Morgan, J., Gergel, S., Coops, N. Aerial photography: a rapidly evolving tool for ecological management. *BioScience.* **2010**, *60*, 47-59.
14. Ambrosia, V., Wegener, S., Zajkowski, T., Sullivan, D., Buechel, S., Enomoto, F., Lobitz, B., Johan, S., Brass, J., Hinkley, E. The Ikhana unmanned airborne system (UAS) western states fire imaging missions: from concept to reality (2006–2010). *Geocarto Int.* **2011**, *26*, 85–101.
15. Watts, A., Ambrosia, V., Hinkley, E. Unmanned aircraft systems in remote sensing and scientific research: Classification and considerations of use. *Remote Sens*. **2012**, *4*, 1671–1692
16. Anderson, K., Gaston, K. Lightweight unmanned aerial vehicles will revolutionize spatial ecology. *Front. Ecol. Environ.* **2013**, *11*, 138–146.
17. Chabot, D., Bird, D. Wildlife research and management methods in the 21st century: Where do unmanned aircraft fit in?. *J. Unmanned Veh. Syst.* **2015**, *3*, 137–155.
18. Linchant, J., Lisein, J., Semeki, J., Lejeune, P., Vermeulen, C. Are unmanned aircraft systems (UASs) the future of wildlife monitoring? A review of accomplishments and challenges. *Mamm Rev*. **2015**, *45*, 239–252.
19. van Gemert, J., Verschoor, C., Mettes, P., Epema, K., Koh, L., Wich, S. Nature conservation drones for automatic localization and counting of animals. *Lect. Notes Comput. Sci.* **2015**, *8925*, 255–270.
20. Hodgson, J., Mott, R., Baylis, S., Pham, T., Wotherspoon, S., Kilpatrick, A., Raja, R., Reid, I., Terauds, A., Koh, L. Drones count wildlife more accurately and precisely than humans. *Methods Ecol. Evol.* **2018**, *9*, 1160-1167.
21. Lhoest, S., Linchant, J., Quevauvillers, S., Vermeulen, C., Lejeune, P. How many hippos (HOMHIP): Algorithm for automatic counts of animals with infra-red thermal imagery from UAV. *Int. Arch. Photogramm. Remote Sens. Spat. Inf. Sci. - ISPRS Arch.* **2015**, 40.
22. Chabot, D., Francis, C. Computer-automated bird detection and counts in high-resolution aerial images: a review. J. Field Ornithol. **2016**, *87*, 343–359.
23. Chen, Y., Shioi, H., Fuentes Montesinos, C., Koh, L., Wich, S., Krause, A. Active Detection via *Adaptive Submodularity. Proceedings of the 31st International Conference on Machine Learning. 2014*, 55–63.
24. Chabot, D. Systematic evaluation of a stock unmanned aerial vehicle (UAV) system for small-scale wildlife survey applications. Master of Science. McGill University, Canada, July 2009.
25. Laliberte, A., Rango, A. Texture and Scale in Object-Based Analysis of Subdecimeter Resolution Unmanned Aerial Vehicle (UAV) Imagery. *IEEE Trans Geosci Remote Sens*. **2009**, *47*, 761-770.
26. Laliberte, A., Ripple, W. Automated Wildlife Counts from Remotely Sensed Imagery. *Wildl. Soc. Bull.* **2003**, *31*, 362–371.
27. Longmore, S., Collins, R., Pfeifer, S., Fox, S., Mulero-Pazmany, M., Bezombes, F., Goodwin, A., De Juan Ovelar, M., Knapen, J., Wich, S. Adapting astronomical source detection software to help detect animals in thermal images obtained by unmanned aerial systems. *Int J Remote Sens.* **2017**, *38*, 2623-2638.

28. Schlatter, R., Salazar, J., Villa, A., Meza, J. Demography of Black-necked swans Cygnus melancoryphus in three Chilean wetland areas. *Wildfowl*. **1991**, *1*, 88–94.
29. BirdLife International. *Cygnus melancoryphus*. The IUCN Red List of Threatened Species. **2016**.
30. Corti, P., Schlatter, P. Feeding Ecology of the Black necked Swan *Cygnus melancoryphus* in Two Wetlands of Southern Chile, *Stud. Neotrop. Fauna Environ*, **2002**, *37*, 9-14.
31. Silva, C., Schlatter, R., Soto-Gamboa, M. Reproductive biology and pair behavior during incubation of the black-necked swan (*Cygnus melanocoryphus*), *Ornitol. Neotrop*. **2012**, *23*, 555-567.
32. Salazar J. Censo poblacional del Cisne de cuello negro (*Cygnus melancoryphus*) en Valdivia. 3er Simposio de Vida Silvestre. *Medio Ambiente*. **1998**. *9*, 78-87.
33. Schlatter, R. (2005). Distribución del cisne de cuello negro en Chile y su dependencia de hábitats acuáticos de la Cordillera de la Costa. En Historia, biodiversidad y ecología de los bosques costeros de Chile, 1st ed.; Smith-Ramírez, C., Armesto, JJ., C. Valdovinos., Eds.; Editorial Universitaria: Santiago, Chile, 2005; pp. 498-504.
34. Polsby, D., Popper, R. The third criterion: Compactness as a procedural safeguard against partisan gerrymandering. *Yale law policy rev*. **1991**, *9*, 301-353.
35. Quantum GIS development team. (2017). Quantum GIS geographic Information System. Open source geospatial foundation proyect.
36. R Core Team. (2017). R: A language and environment for statistical computing. R Foundation for Statistical computing, Vienna, Austria
37. Hijmans, R. (2016a). raster: Geographic Data Analysis and Modeling, R package version 2.5-8
38. Bivand, R., Keitt, T., Barry, R. (2017). rgdal: Bindings for the Geospatial Data Abstraction Library, R package version 1.2-8.
39. Hijmans, R. (2016b). geosphere: Spherical Trigonometry, R package version 1.5-5.
40. Baddeley, A., Turner, R. spatstat: An R Package for Analyzing Spatial Point Patterns, *J. Stat. Softw.* 2005, *12*, 1-42.
41. Bivand, R., Lewin-Koh, N. (2017) maptools: Tools for Reading and Handling Spatial Objects, R package version 0.9-2.
42. Greenberg, J., Mattiuzzi, M. (2015). gdalUtils: Wrappers for the Geospatial Data Abstraction Library (GDAL) Utilities, R package version 2.0.1.7.
43. Bivand, R., Rundel, C. (2017). rgeos: Interface to Geometry Engine - Open Source (GEOS), R package version 0.3-23.
44. Evans, J. (2017) spatialEco, R package version 0.0.1-7
45. Bengtsson, H. (2016). R.utils: Various Programming Utilities. R package version 2.5.0
46. Ruuska, S., Hämäläinen, W., Kajava, S., Mughal, M., Matilainen, P., Mononen, J. Evaluation of the confusion matrix method in the validation of an automated system for measuring feeding behaviour of cattle. *Behav. Processes.* **2018**, *148*, 56-62.
47. Aniceto, A., Biuw, M., Lindstrøm, U., Solbø, S. A., Broms, F., Carroll, J. Monitoring marine mammals using unmanned aerial vehicles: quantifying detection certainty. *Ecosphere.* **2018**, *9*, e02122.
48. Chabot, D., Craik, S., Bird, D. Population census of a large common tern colony with a small unmanned aircraft. *PLoS One* **2015**, *10*, e0122588.
49. Mader, S., Grenzdörffer, G. Automatic Sea bird detection from high resolution aerial imagery. *Int. Arch. Photogrammetry, Remote Sens. Spatial Inf. Sci*. **2016**, *41*, 299-303.
50. Goebel, M., Perryman, W., Hinke, J., Krause, D., Hann, N., Gardner, S., LeRoi, D. A small unmanned aerial system for estimating abundance and size of Antarctic predators. *Polar Biol.* **2015**, *38*, 619-630.
51. Hodgson, J., Baylis, S., Mott, R., Herrod, A., Clarke, R. H. (2016). Precision wildlife monitoring using unmanned aerial vehicles. *Sci. Rep.* **2016**, *6*, 1-7.
52. Brack, I., Kindel, A., Oliveira, L. Detection errors in wildlife abundance estimates from Unmanned Aerial Systems (UAS) surveys: Synthesis, solutions, and challenges. *Methods Ecol evol.* **2018**, *9*, 1864-1873.
53. Garner, D., Underwood, H., Porter, W. Use of modern infrared thermography for wildlife population surveys. *Environ Manage.* **1995**, *19*, 233-238.
54. Franke, U., Goll, B., Hohmann, U., Heurich, M. Aerial ungulate surveys with a combination of infrared and high–resolution natural colour images. *Anim Biodivers Conserv*. **2012**, *35*, 285-293.
55. Chrétien, L., Théau, J., Ménard, P. Visible and thermal infrared remote sensing for the detection of white-tailed deer using an unmanned aerial system. *Wildl. Soc. Bull.* **2016**, *40*, 181-191.
56. Brack, I., Kindel, A., Oliveira, L. Detection errors in wildlife abundance estimates from Unmanned Aerial Systems (UAS) surveys: Synthesis, solutions, and challenges. *Methods Ecol evol.* **2018**, *9*, 1864-1873.
57. Flores-de-Santiago, F., Valderrama-Landeros, L., Rodríguez-Sobreyra, R., Flores-Verdugo, F. Assessing the effect of flight altitude and overlap on orthoimage generation for UAV estimates of coastal wetlands. *J. Coast. Conserv.* **2020**, *24*, 1-11.
58. Chrétien, L., Théau, J., Ménard, P. Wildlife multispecies remote sensing using visible and thermal infrared imagery acquired from an unmanned aerial vehicle (UAV). *Int. Arch. Photogramm. Remote Sens. Spat. Inf. Sci. - ISPRS Arch*. **2015**, *40*.
59. Seymour, A. Dale, M. Hammill, P. Halpin, Johnston, D. Automated detection and enumeration of marine wildlife using unmanned aircraft systems (UAS) and thermal imagery. Sci. Rep. 2017, 7, 1– 10.